PAPER

Check for updates

A dragon fruit peel-derived heterogeneous catalyst for Michael addition reactions and methanolysis of PET waste: a green and dual-functional approach

Vanlalngaihawma Khiangte, [ID] †[ab] Samson Lalhmangaihzuala,†[a] Z. T. Laldinpuii[ab] and Khiangte Vanlaldinpuia [ID] *[a]

In this study, we investigate the innovative use of a low-cost dragon fruit peel-derived heterogeneous catalyst for two environmentally significant reactions: the Michael addition reactions and the methanolysis of PET waste. For the Michael addition reaction, optimal conditions were found to be 10 wt% DFPA catalyst with 0.5 mL ethyl acetate, achieving maximum conversion within 15 min. We systematically studied this transformation using three Michael donors – acetylacetone, ethyl acetoacetate, and malononitrile – and six β-nitrostyrene derivatives as acceptors. In the methanolysis of PET waste, central composite design-based response surface methodology (RSM) was employed for optimization. Statistical analysis confirmed the significance of the design experiment, with optimized conditions of 36.29 mg catalyst loading, 0.97 h reaction time, 5.7 mL methanol, and 204 °C reaction temperature, yielding 98.64% dimethyl terephthalate. The catalyst demonstrated good to excellent reusability, maintaining an 84.56% DMT yield even after the tenth cycle. Michael products were all confirmed using NMR analysis, and HPLC, FT-IR, and NMR analyses were employed for DMT confirmation.

Environmental significance

Polyethylene terephthalate (PET), a non-biodegradable thermoplastic polymer, poses a growing environmental concern due to its widespread use in single-use packaging. While plastic pollution is widespread on land, marine environments reflect the global scale of the crisis. An estimated 14 million tons of plastic waste enter the oceans annually, with PET comprising a significant portion. Addressing this dilemma requires more than a simple ban; it demands a complete system redesign of the economy to mitigate human impact and ensure a sustainable future. Researchers in the field increasingly embrace catalysts that originate from natural sources, such as biomass, due to their non-toxicity, low corrosiveness, and cost-effectiveness. This study explores dragon fruit peel ash (DFPA), a biomass-derived, eco-friendly catalyst, for methanolysis of PET waste and Michael addition reactions, offering a low-cost, sustainable approach to waste valorization. The utilization of biomass waste DFPA presents a compelling solution to the challenges posed by expensive catalyst systems, while simultaneously promoting waste valorization through the integration of biomass waste and PET waste, alongside the development of environmentally friendly methodologies in synthetic transformations.

1. Introduction

In recent decades, the natural environment has witnessed a significant buildup of biomass waste, largely driven by rapid population growth, intense economic development, and accelerated industrialization.[1] The rising demand for food, housing, and energy drives the expansion of agricultural, forestry, and livestock activities, thereby generating substantial quantities of organic waste, such as crop residues, animal manure, food leftovers, and wood waste.[2,3] Economic progress further amplifies this trend by modernizing agricultural and food processing systems, resulting in even more organic byproducts. If not properly managed, biomass waste can have serious environmental consequences.[4–6] Decomposing organic matter releases methane, a potent greenhouse gas that significantly contributes to climate change.[7] Untreated animal and agricultural waste pollutes water bodies, and open burning of crop residues leads to air pollution and soil degradation.[8–10] Additionally, the accumulation of food and animal waste emits foul odors, posing health risks to surrounding communities.[11]

However, converting biomass waste into valuable products like useful materials and energy offers an environmentally sustainable solution that can greatly decrease pollution, minimize landfill waste, and reduce our dependence on fossil fuels.[12] For example, composting transforms food and agricultural residues into nutrient-rich organic fertilizer, while anaerobic digestion generates biogas along with a fertilizing byproduct known as digestate.[13,14] When biomass is heated under low-oxygen conditions, it produces biochar – a carbon-

aDepartment of Chemistry, Pachhunga University College, Mizoram University, Aizawl, Mizoram, 796001, India. E-mail: mapuiakhiangte@pucollege.edu.in

bDepartment of Chemistry, Mizoram University, Aizawl, Mizoram, 796001, India

† These authors contributed equally.

dense material that enhances soil health and sequesters carbon.[15] Biomass can also serve as a source for producing bio-fuels and renewable energy, helping to cut down greenhouse gas emissions.[5] Furthermore, certain types of biomass can be repurposed into biodegradable plastics, bio-based chemicals, and various other industrial products.[16]

In recent years, significant progress in materials research has led to the development of waste-inspired heterogeneous catalysts that are cost-effective, safer, and more affordable, providing an innovative solution to the solid waste disposal problem and reducing the potential risk of foreseeable environmental pollution.[17,18] Recent advancements in the exploitation of waste biomass have generated a robust foundation for the promotion of biodiesel production,[19,20] carbon–carbon bond formation,[21,22] and upcycling of plastic waste.[23–25] In addition, the synthesis of biomass waste-derived quantum dots also presents opportunities for diverse applications.[20,26] Herein, as part of our ongoing project, we have investigated the catalytic activity of dragon fruit peel ash (DFPA) for catalyzing the methanolysis of waste polyethylene terephthalate (PET) and the C–C bond-forming Michael addition reaction.[27] Although dragon fruit peel ash was employed in this study, the catalyst preparation method is applicable to other biomass-derived ashes with comparable compositions, such as those obtained from banana,[28] orange,[22] or mango peels,[29] demonstrating the method's universality and sustainability. However, only those that contain an adequate concentration of the active site can effectively function as catalysts. Therefore, further exploration and identification of such biomass-derived materials are essential, as they are renewable, cost-effective, environmentally benign, and readily available.

As per reported statistics, the global production of polyethylene terephthalate (PET) has surpassed 30 million tons, representing approximately 13% of the total annual plastic output.[30] The extensive application of the materials, confined to their single use as well as their remarkable durability against natural deterioration, has resulted in the vast buildup of waste PET.[31,32] Over half of global PET waste ends up in landfills, comprising about 12% of the world's solid waste volume.[33–35] Therefore, the conversion of waste plastics into value-added products has garnered significant attention in recent scientific investigations. While glycolysis has consistently proven to be the most cost-effective and economically feasible chemical recycling technique, methanolysis exhibits a higher level of tolerance to contaminants.[36] This characteristic enables methanolysis to effectively depolymerize low-grade feedstocks, thereby significantly reducing the overall cost of raw materials.[36] The complete methanolysis of PET to the monomer dimethyl terephthalate (DMT) has often been studied and reviewed. While different varieties of catalysts were employed, raw biowaste as a source of heterogeneous catalysts emerged as a promising candidate. Their alignment with the 'Principles of Green Chemistry' is evident,[37] as they offer a non-hazardous, easy preparative step and a low-cost alternative to complex synthetic catalysts. The significance of recycling waste plastics and our continuous focus on waste-derived heterogeneous catalysts led us to explore the methanolysis of post-consumed PET bottles.

In the meantime, the Michael addition reaction is a well-established and reliable synthetic protocol for forming carbon–carbon bonds in organic synthesis.[38–40] Among different variants of nucleophilic addition reactions, the reaction of carbonyl compounds with electron-deficient nitroolefins has received particular attention.[41–43] This approach has gained popularity due to the easy accessibility and remarkable reactivity of nitroalkenes, along with the valuable synthetic applications of the resulting nitroalkane Michael adducts.[44,45] Although there have been a number of reports in the area, the utilization of heterogeneous catalysts derived from waste biomass is uncommon and remains limited, with only a handful of examples documented in the literature. Furthermore, in light of the progressive advancements of the concept 'green and sustainable chemistry,' the exploration of environmentally benign methodologies for the efficient formation of C–C bonds continues to garner considerable attention within the scientific community.

2. Materials and methods

2.1. Materials

Nitrostyrenes, acetylacetone, ethyl acetoacetate, and malononitrile were procured from Sigma-Aldrich, and PET bottles and dragon fruit peels were acquired from a local shop and Green Wave Farmtech, respectively, at Aizawl, Mizoram, India. The PET bottles were washed, dried, and cut into 1–2 mm PET flakes. Laboratory-synthesized distilled water was used, and methanol was obtained from Merck, India.

2.2. Catalyst preparation and characterization

As part of our ongoing research on the utilization of dragon fruit peel ash-derived heterogeneous catalysts (DFPAs), the previously reported DFPA catalyst was further employed in methanolysis of PET waste and Michael addition reactions. The synthesis and detailed characterization of the catalyst have been reported in our earlier publication,[27] and the summarized data are provided in the SI, along with the additional Temperature-Programmed Desorption (TPD) analysis. It involves several steps: the raw biomass was washed thoroughly to remove impurities and then broken down into smaller pieces. It was subsequently dried to eliminate moisture content and subjected to open-air combustion to produce the ash. The resulting ash was finally sieved to obtain a fine, uniform solid material, which was used as the ash-based catalyst. The catalyst was then characterized using different techniques such as X-ray Diffraction (XRD), X-ray Photoelectron Spectroscopy (XPS), X-ray Fluorescence (XRF), Energy Dispersive X-ray (EDX), Thermogravimetric Analysis (TGA), Temperature-Programmed Desorption (TPD), Fourier Transform Infrared Spectroscopy (FTIR), Brunauer–Emmett–Teller (BET), Surface Electron Microscopy (SEM), and Transmission Electron Microscopy (TEM). Confirmation of the desired product was done using High Performance Liquid Chromatography (HPLC), FT-IR analyses, and Nuclear Magnetic Resonance spectroscopy (NMR).

© 2026 The Author(s). Published by the Royal Society of Chemistry

Environ. Sci.: Adv., 2026, **5**, 192–205 | 193

2.3. General procedure for the Michael addition reaction

For a typical reaction, 1 mmol of acetylacetone dissolved in 5.12 eq. of ethyl acetate (EtOAc) was allowed to react with 1.2 eq. of trans-β-nitrostyrene in the presence of 10 wt% DFPA catalyst at room temperature. Thin-layer chromatography (TLC) was employed to monitor the progress of the reaction, and 10 mL of ethyl acetate was added after completion of the reaction. The catalyst was then recovered by filtration using filter paper and subsequently washed with ethyl acetate to ensure complete product isolation. Solvent extraction was then performed twice with distilled water (2 × 20 mL) to remove any unwanted impurities, and anhydrous Na_2SO_4 was used to dry out the organic layer from moisture. The crude product was purified by silica gel column chromatography with an ethyl acetate/hexane (1 : 4) mixture as the eluent. The product's yield percentage was determined using eqn (1), and its confirmation was achieved through NMR analysis.

$$\text{Yield (\%)} = \frac{\text{isolated yield}}{\text{theoretical yield}} \times 100 \tag{1}$$

2.4. General procedure of the methanolysis reaction, leaching test, and reusability of the catalyst

In a 50 mL Teflon-lined hydrothermal autoclave, 2.6 mmol (0.5 g) of PET flakes was allowed to react with 5 mL of methanol in the presence of 30 mg of DFPA catalyst at 204 °C for 0.97 h. The autoclave temperature was brought down to room temperature after a given reaction time, and the catalyst was separated through filter paper and washed with 40 mL of hot methanol. The filtrate was then brought down to room temperature and placed in a refrigerator set at 2 °C. A white, crystalline dimethyl terephthalate (DMT) solid was formed, and the filtrate was decanted to isolate the recrystallized DMT. The filtrate was then stirred for approximately 30 min to allow the separation of other by-products, followed by filtration through filter paper. The remaining filtrate was then further processed through an ethylene glycol and methanol recovery process under reduced pressure. The percentage yield was determined using eqn (2), and the recrystallized product was then subjected to NMR and HPLC analysis to confirm the synthesis of the intended product and its purity.

$$\text{Yield\%} = \frac{\text{recrystallized yield}}{\text{theoretical yield}} \times 100 \tag{2}$$

To investigate the catalyst heterogeneity, the same amount of reaction component was first charged into the reactor without PET, and the reaction was run for 0.5 h at 204 °C. The autoclave was cooled, and the catalyst was separated out using filter paper. 0.5 g of PET was added to the methanol solution containing the leach component and run for another 0.97 h. The methanol filtrate was generated twice for ICP-OES analysis. Finally, the reactor was cooled and checked for any PET conversion as discussed above. For environmental considerations, the generated ethylene glycol and residual methanol were recovered under reduced pressure, while the residues formed during the experiments were collected

Table 1 Experimental variables of methanolysis and their corresponding levels

Name	Code	Units	−α	Low	0	High	+α
Catalyst loading	A	mg	10	20	30	40	50
Methanol loading	B	mL	1	3	5	7	9
Reaction time	C	h	0.25	0.5	0.75	1	1.25
Reaction temperature	D	°C	180	190	200	210	220

and subjected to re-depolymerization using the same protocol to ensure complete conversion of depolymerizable intermediates and unreacted PET to DMT, thereby enhancing the environmental sustainability of the process. The residual non-convertible byproducts, which were minimal, were disposed of in a landfill. The reusability of the catalyst was also investigated under the optimized reaction conditions. In each cycle, the PET loading and the corresponding amounts of other reaction components were adjusted according to the recovered catalyst quantity. The elemental composition and morphological change of the catalyst after the 5th and 10th cycles were examined using SEM-EDX analysis.

2.5. Design of experiment for methanolysis of PET waste

Response surface methodology serves as a statistical tool for enhancing the accuracy of the optimization process of a reaction. So, the experimental optimization process of the methanolysis of PET waste was designed and modeled with the inbuilt central composite design (CCD) variant response surface methodology in Design Expert 13 software. Four independent variables were studied as shown in Table 1, and their levels were determined using a preliminary reaction and literature survey. The input variables and their levels then generated thirty experiments, including 16 factorial points, 8 axial points, and 6 central points that were experimented with and statistically evaluated using the built-in ANOVA (analysis of variance) technique. A quadratic polynomial eqn (3) was employed to study the interaction between the experimental result and the independent variables, where Y, k, and ε denote the response, the number of factors, and the error, X_i and X_j are independent variables, and i and j are integer variables. β_0, β_i, β_{ii}, and β_{ij} are the coefficients of intercept, linear, quadratic, and interaction between i and j, respectively.

$$Y = \beta_0 + \sum_{i=1}^{k} \beta_i X_i + \sum_{i=1}^{k} \beta_{ii} X_i^2 + \sum_{i=1}^{k} \sum_{j=1}^{k} \beta_{ij} X_i X_j + \varepsilon \tag{3}$$

3. Results and discussion

3.1. Optimization of the Michael addition reaction using DFPA

The Michael addition reaction was first conducted with acetylacetone and trans-β-nitrostyrene in the absence of solvent to study the catalyst activity. The catalyst helped to promote the reaction to a certain extent, but it solidified and could not be further processed, yielding just 28% of the desired product
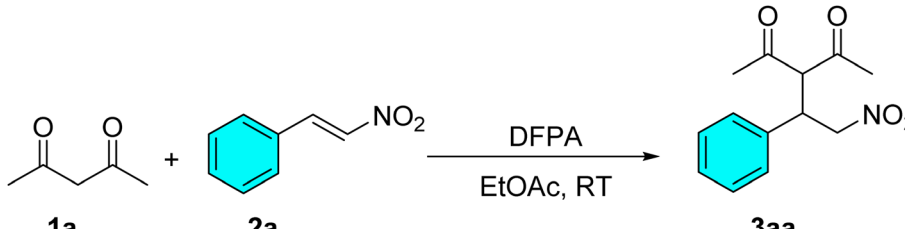
(Table 2, entry 1). The reaction was then optimized using different solvents, starting from the protic solvent, as shown in Table 2, entries 2–7. When the reaction was performed with 0.5 mL of water and ethanol, only a trace amount of the product was observed due to the formation of a side product that is soluble in water.[46,47] Table 2, entries 4–10 demonstrate that using acetonitrile as a solvent extended the reaction time to 1.5 h, whereas employing dichloromethane (DCM), ethyl acetate (EtOAc), and dimethyl sulfoxide (DMSO) reduced it significantly to 20, 15, and 25 min, respectively. Based on these results, 0.5 mL of EtOAc, a greener alternative to many traditional solvents due to its biodegradability and low toxicity, was selected as the optimal solvent for the reaction.

The investigation into catalyst loading, ranging from 5 to 20 wt%, was then carried out in relation to reaction time and yield. As seen in Table 2, entries 7 and 11–13, full conversion was accomplished in every trial with negligible yield differences but discernible variations in response time. Increasing the catalyst loading from 5 wt% to 10 wt% enhanced the reaction rate, reducing the time from 30 min to 15 min. However, further increasing the catalyst loading beyond 10 wt% led to a decline in the reaction rate, as the mixture became slurry-like, potentially hindering mass transfer and catalyst efficiency. Therefore, a catalyst loading of 10 wt% was sufficient to achieve complete conversion in the shortest reaction time.

The loading of reactants was further adjusted to optimize the reaction conditions. Given that the polarity of nitrostyrene is lower than that of the reactants and is closer to that of the products, Michael donors (acetylacetone, ethyl acetoacetate, and malononitrile) were used as limiting reactants. This approach aimed to achieve pure and complete isolation of the product, as demonstrated in Table 2, entries 7 and 14–16. An incomplete conversion of acetylacetone was observed through TLC when equimolar concentration and 0.8 eq. were used in the reaction, and thus only 84% and 71% yields were isolated, respectively (entries 15 and 16). Conversely, full conversion was achieved when 1.2 and 1.4 eq. were used in the reaction with no significant change in the yield, as shown in entries 4 and 13. Therefore, 1.2 eq. was used for performing the Michael addition reaction, and the isolated products were confirmed using ^{1}H and ^{13}C NMR analysis as detailed in the SI. Henceforth, the ideal reaction conditions were found to be 1.2 eq. of *trans*-β-nitrostyrene, 10 wt% DFPA catalyst, and 0.5 mL (7.83 eq.) of DCM at room temperature (Table 2, entry 4).

Upon the establishment of the optimized reaction conditions (Table 2, entry 7), we proceeded to investigate the scope and generality of the catalytic system for Michael addition of acetylacetone, ethyl acetoacetate, and malononitrile with different nitrostyrene derivatives for the synthesis of nitro-alkane compounds (Table 3). During the experimentation, a series of substituted aromatic nitrostyrenes bearing electron-
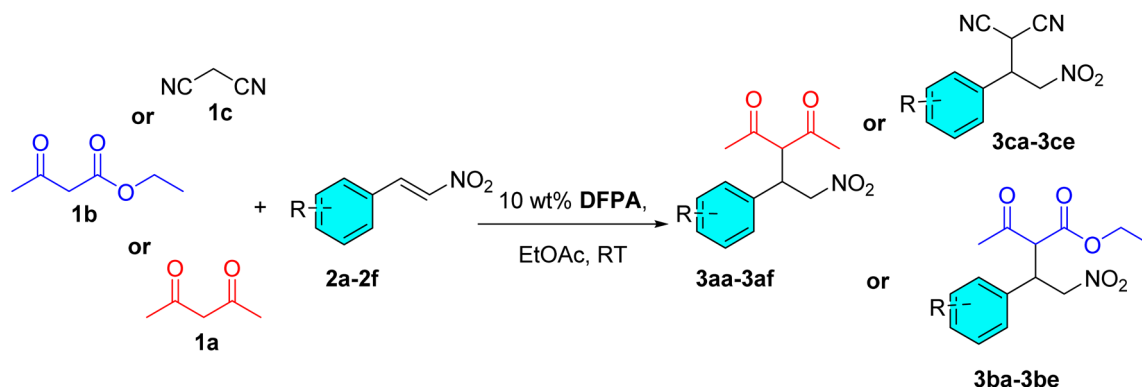
Table 2 Optimization of the DFPA promoted Michael addition reaction[a]

Sl. no.	Solvent (mL)	Catalyst (wt%)	**2a** (eq.)	Time (min)	Yield[b] (%)
1	Neat	10	1.2	20	28 ± 1.2
2	H$_2$O (0.5)	10	1.2	180	Trace
3	EtOH (0.5)	10	1.2	180	Trace
4	DCM (0.5)	10	1.2	20	95 ± 1.4
5	DMSO (0.5)	10	1.2	25	91 ± 1.6
6	CH$_3$CN (0.5)	10	1.2	90	90 ± 0.8
7	**EtOAc (0.5)**	**10**	**1.2**	**15**	**95 ± 1.5**
8	EtOAc (0.25)	10	1.2	22	91 ± 1.3
9	EtOAc (0.75)	10	1.2	23	93 ± 1.4
10	EtOAc (1)	10	1.2	24	94 ± 1.6
11	EtOAc (0.5)	5	1.2	30	89 ± 1.7
12	EtOAc (0.5)	15	1.2	22	91 ± 1.4
13	EtOAc (0.5)	20	1.2	25	93 ± 1.2
14	EtOAc (0.5)	10	1.4	15	94 ± 1.7
15	EtOAc (0.5)	10	1	15	84 ± 1.8
16	EtOAc (0.5)	10	0.8	15	71 ± 1.5

[a] Reaction conditions: 1 mmol of acetylacetone and stated amounts of *trans*-β-nitrostyrene, solvent, and DFPA catalyst at room temperature. [b] Isolated yield.

© 2026 The Author(s). Published by the Royal Society of Chemistry

Environ. Sci.: Adv., 2026, **5**, 192–205 | **195**

Table 3 Michael addition reaction of acetyl acetone, ethyl acetoacetate and malononitrile with various nitrostyrenes[a]

Sl. no.	Donors	R	Product	Time (min)	Yield[b] (%)	SD[c]
1	**1a**	H (**2a**)	**3aa**	15	95 ± 1.4	0.71
2	**1b**	H (**2a**)	**3ba**	10	93 ± 0.8	0.4
3	**1c**	H (**2a**)	**3ca**	40	94 ± 1.2	0.6
4	**1a**	p-Br (**2b**)	**3ab**	10	94 ± 1.8	0.90
5	**1b**	p-Br (**2b**)	**3bb**	10	92 ± 1.9	0.99
6	**1c**	p-Br (**2b**)	**3cb**	30	92 ± 1.6	0.82
7	**1a**	o-Cl (**2c**)	**3ac**	15	92 ± 1.5	0.81
8	**1b**	o-Cl (**2c**)	**3bc**	10	94 ± 1.3	0.63
9	**1c**	o-Cl (**2c**)	**3cc**	35	89 ± 1.1	0.57
10	**1a**	p-Cl (**2d**)	**3ad**	10	92 ± 1.3	0.71
11	**1b**	p-Cl (**2d**)	**3bd**	10	89 ± 1.7	0.91
12	**1c**	p-Cl (**2d**)	**3cd**	25	90 ± 1.4	0.71
13	**1a**	p-CH$_3$ (**2e**)	**3ae**	25	90 ± 1.9	1.04
14	**1b**	p-CH$_3$ (**2e**)	**3be**	20	94 ± 1.8	0.92
15	**1c**	p-CH$_3$ (**2e**)	**3ce**	50	92 ± 1.4	0.72
16	**1a**	o-OCH$_3$ (**2f**)	**3af**	30	93 ± 1.5	0.81
17	**1a**	H (**2a**)	—	15	97 ± 1.6[d]	0.83
18	**1b**	H (**2a**)	—	10	95 ± 0.9[d]	0.45
19	**1c**	H (**2a**)	—	38	95 ± 1.2[d]	0.61

[a] General reaction conditions: Michael addition reaction was conducted in triplicate with 1 mmol of **1** and 1.2 eq. of **2** in the presence of 10 wt% DFPA catalyst and 0.5 mL EtOAc at room temperature. [b] Isolated yield. [c] Standard deviation. [d] One gram-scale reaction.

donating, electron-withdrawing, and neutral functional groups was investigated. Regardless of the electronic nature or positional variation of the substituents on the aromatic ring, the reactions proceeded smoothly to give the desired adducts in consistently high yields (up to 95%, Table 3, entry 1) in a short period of reaction duration. A gram-scale reaction was then performed using *trans*-β-nitrostyrene with all three Michael donors (Table 3, entries 17–19) to demonstrate the practicality of the reaction on a larger scale. The results showed full conversion, a higher isolated yield for each donor, and no significant changes in the reaction duration. These findings highlight the robustness and efficiency of the catalytic system, which appears to tolerate a broad range of electronic environments. Moreover, the minimal variation observed across the substrate scope suggests that the steric and electronic properties of the nitrostyrene moiety exert only a limited influence on the overall transformation, thereby demonstrating the general applicability and sustainability of this protocol for the synthesis of structurally diverse nitroalkane adducts.

4. Green metrics and plausible reaction mechanism of the Michael addition reaction using DFPA

The *E*-factor green metric was found to be 0.22, indicating that only 0.22 kg of waste will be generated per kilogram of Michael adduct produced. The process mass intensity of 1.22 reflects a highly efficient process, with the PMI approaching the ideal value. Meanwhile, as shown in Fig. 1, the Michael addition reaction is initiated by the abstraction of a proton from an active methylene substrate through surface oxide (O^{2-}) species of K_2O, CaO, MgO, *etc.*, present in the DFPA catalyst, generating an enolate intermediate. This enolate then attacks the β-carbon of the nitrostyrene through 1,4-conjugate addition with its nucleophilicity, resulting in the formation of a new C–C bond. The α carbon of the nitrostyrene moiety then subsequently abstracted an available proton from the catalyst surface-bound OH^- group that originates from the deprotonation step through conjugation from the nitro group. This process generates the
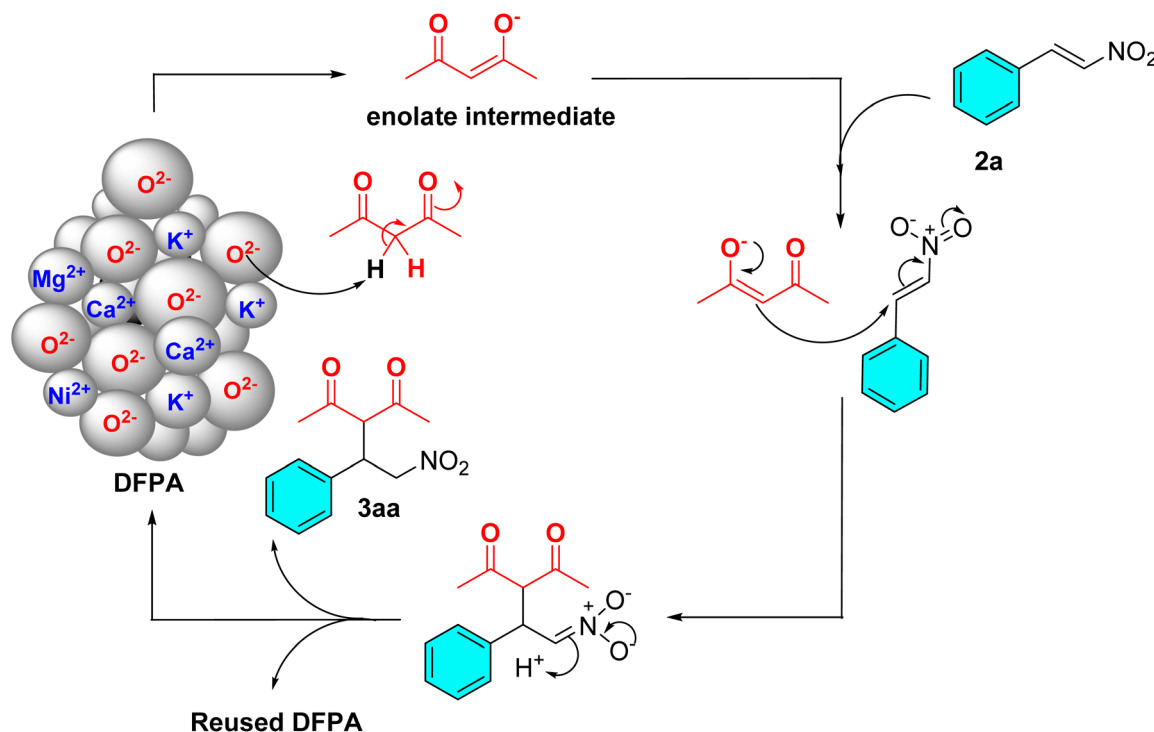
Fig. 1 Plausible reaction mechanism of the Michael addition reaction between acetyl acetone and *trans*-β-nitrostyrene.

Michael product and simultaneously regenerates the active O^{2-} site of the catalyst, thereby enabling a repeatable catalytic cycle.

5. Optimization of methanolysis of PET waste using DFPA

5.1. Statistical result of CCD-based response surface methodology

The experimental data of the generated experiments were incorporated into Design Expert software as shown in Table 4, and the analysis was performed with the given data to determine and evaluate the regression model and statistical significance. The fit summary suggests a quadratic polynomial equation with $R^2 = 0.9743$, and a coded second-order polynomial eqn (4) was utilized to obtain the predicted response. The coded factors A, B, C, and D are catalyst loading, methanol loading, reaction time, and temperature, respectively, and the predicted yields are shown in Table 4. The probability value ($p = <0.0001$) and Fischer's test value ($F = 40.69$) of the model determine the suitability of the quadratic regression model at the 95% confidence level, as there is only a 0.01% chance that this large F-value can arise from noise, and a p-value below 0.05 denotes the model's significance. Accordingly, the variables and interaction of A, B, C, D, BD, A^2, B^2, C^2, and D^2 are significant as shown in Table 5. The insignificant lack of fit with a p-value of 0.0679 also indicates that the experimental data fitted successfully to study the effect of variable factors in the regression response.[28,48] The accessibility of the regression model equation can also be seen from the predicted R^2 (0.8644) and adjusted R^2 (0.9504), as their deviation is less than 0.2 as shown in Table 6. The adequate precision also supplemented the significance of the model, showing a reasonably high signal-to-noise ratio of 20.5574, which is above the desirable signal-to-noise ratio (>4). The lower standard deviation of 1.54 and the coefficient of variation percent (CV%) of 1.73% further signify the close relationship between the experimental and predicted yield, where <10% CV% is desirable.[49] From Fig. 2a, b and S28b showing the predicted *vs.* actual graph, normal probability plot of residuals, and externally studentized *vs.* run, we also concluded that the actual yield closely aligns with the predicted yield, the residual errors are distributed along a straight line within a narrow range, and no externally studentized residuals exceeded ±3 (ranging from −2.354 to 2.476), showing the absence of outliers, respectively. This indicates the reliability and significance of the experimental input data. Moreover, the leverage value of all the factorial, axial, and center point runs was well below the threshold value of 1, as shown in the leverage *vs.* run plot (Fig. S25a), confirming the reliability of the experimental data for model fitting.

$$\begin{aligned} \text{Yield} = {} & 97.86 + 1.53A + 1.79B + 3.34C + 3.13D - 0.0481AB \\ & + 0.5894AC - 0.3219AD - 0.3031BC \\ & - 0.9319BD - 0.1194CD - 1.98A^2 \\ & - 2.40B^2 - 2.90C^2 - 4.03D^2 \end{aligned} \tag{4}$$

5.2. Interaction study of input variables

The 3D surface model plot was employed to study the impact of interaction between four independent variables, A, B, C, and D, on the depolymerization of PET waste. Fig. 3a shows the effect

© 2026 The Author(s). Published by the Royal Society of Chemistry

Environ. Sci.: Adv., 2026, **5**, 192–205 | **197**

Table 4 Experimental design and the corresponding responses[a]

Polyethylene terephthalate (PET) → (10 wt% DFPA, 200 °C, 5 ml CH$_3$OH) → Dimethyl terephthalate (DMT) + Ethylene glycol

Run	A: catalyst loading (mg)	B: MeOH loading (mL)	C: reaction time (h)	D: reaction temp. (°C)	Yield[b] (%)	Predicted yield (%)
1	30	5	0.75	200	97.99	97.86
2	30	5	0.75	200	98.86	97.86
3	30	5	1.25	200	93.75	92.95
4	30	1	0.75	200	82.97	84.66
5	40	7	1	210	94.74	95.22
6	20	3	1	190	83.75	81.96
7	30	5	0.75	180	73.44	75.49
8	30	5	0.75	220	90.15	88.03
9	30	5	0.25	200	78.85	79.58
10	40	7	0.5	190	84.65	84.20
11	20	3	0.5	190	75.55	75.61
12	20	3	0.5	210	86.04	84.62
13	40	3	1	210	93.63	94.20
14	30	5	0.75	200	97.76	97.86
15	20	7	1	210	90.82	91.71
16	40	7	0.5	210	86.87	88.20
17	50	5	0.75	200	93.54	93.00
18	40	7	1	190	90.74	91.69
19	40	3	0.5	210	85.67	85.97
20	20	7	1	190	86.66	86.90
21	40	3	1	190	87.6	86.95
22	30	5	0.75	200	96.69	97.86
23	20	7	0.5	210	85.86	87.05
24	20	7	0.5	190	82.79	81.76
25	40	3	0.5	190	79.59	78.24
26	10	5	0.75	200	86.39	86.86
27	30	5	0.75	200	98.79	97.86
28	30	5	0.75	200	97.06	97.86
29	20	3	1	210	89.51	90.50
30	30	9	0.75	200	93.59	91.83

[a] 2.6 mmol of PET flakes was used for this optimization. [b] Percentage of recrystallized yield.

of varying catalyst and methanol loadings on the reaction at constant temperature (200 °C) and time (0.75 h). Both show significant changes as the catalyst's active site and available reactants have increased while raising their concentration. However, as seen in the 3D plots, the yield percentage of DMT declines with an increased dosage of catalyst and methanol beyond ∼34 mg and ∼5.7 mL, which could be due to the attainment of a reversible reaction that leads to the formation of oligomers.[50]

Similarly, the increase in reaction time and catalyst loading at constant temperature (200 °C) and methanol dosage (5 mL) also positively influences the DMT yield until it reaches ∼0.9 h reaction time and ∼34 mg catalyst loading, as shown in Fig. 3b. This could be due to the formation of other depolymerized products.[22]

In Fig. 3c, the effect of catalyst loading and reaction temperature is presented, while keeping the methanol dosage and reaction time constant at 5 mL and 0.75 h, respectively. The DMT yield shows a positive trend up to around 34 mg catalyst loading and 204 °C, which can be explained by enhanced catalytic activity at elevated temperatures and higher catalyst concentrations. A subsequent decline in yield is observed, likely due to the onset of the reverse reaction or oligomer formation.[22]

Moreover, the effect of reaction time and methanol loading on the DMT yield at constant temperature (200 °C) and catalyst loading (30 mg) is displayed in Fig. 3d. As shown in the 3D graph. The yield progressively rises as the reaction time and methanol concentration are increased to ∼0.9 h and ∼5.7 mL, respectively, beyond which a reversible reaction might be achieved as the DMT yield declines.

Table 5   ANOVA results of methanolysis of PET waste

Source	Sum of squares	df	Mean square	F-Value	p-Value	
Model	1349.16	14	96.37	40.69	<0.0001	Significant
A-Catalyst loading	56.46	1	56.46	23.84	0.0002	
B-Methanol loading	77.15	1	77.15	32.58	<0.0001	
C-Reaction time	268.20	1	268.20	113.25	<0.0001	
D-Reaction temperature	235.81	1	235.81	99.58	<0.0001	
AB	0.0371	1	0.0371	0.0156	0.9021	
AC	5.56	1	5.56	2.35	0.1463	
AD	1.66	1	1.66	0.7000	0.4159	
BC	1.47	1	1.47	0.6208	0.4430	
BD	13.89	1	13.89	5.87	0.0286	
CD	0.2280	1	0.2280	0.0963	0.7606	
A^2	107.81	1	107.81	45.53	<0.0001	
B^2	158.50	1	158.50	66.93	<0.0001	
C^2	230.49	1	230.49	97.33	<0.0001	
D^2	444.38	1	444.38	187.65	<0.0001	
Residual	35.52	15	2.37			
Lack of fit	31.62	10	3.16	4.05	0.0679	Not significant
Pure error	3.90	5	0.7801			
Cor total	1384.68	29				

Table 6   FIT statistics of ANOVA

Std. dev.	1.54	R^2	0.9743
CV%	1.73	Adjusted R^2	0.9504
Adeq. precision	20.5574	Predicted R^2	0.8644

Similarly, Fig. 3e shows the effect of methanol concentration and reaction temperature on the DMT yield at constant reaction time (0.75 h) and catalyst loading (30 mg). The DMT yield first increased with an increase in methanol concentration and reaction temperature and declined after reaching around 5.6 mL and ~203 °C due to the formation of oligomers that are insoluble in water.

Furthermore, the 3D plot of Fig. 3f demonstrated how temperature and reaction time influence the DMT yield at a constant catalyst (30 mg) and methanol loading (5 mL). The DMT yield increases with an increase in both the parameters, maximized at ~0.9 h and ~204 °C, and declines thereafter. Notably, across most interaction plots, the DMT yield shows only marginal variation near the peak values, indicating that the system approaches optimal conditions. Nevertheless, further optimization of the reaction parameters is required to obtain the exact optimum conditions for achieving maximum DMT yield.

5.3. Optimization of reaction parameters and characterization of the methanolysis product

The numerical optimization tool was implemented to determine the optimal conditions for the depolymerization of PET to DMT using a DFPA catalyst. The software predicted a maximum
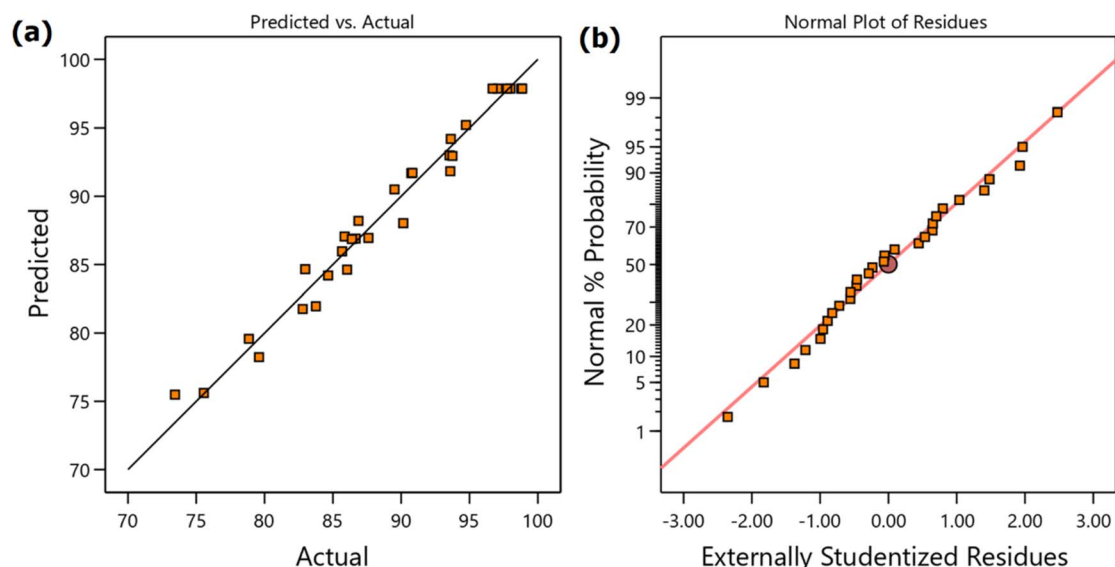

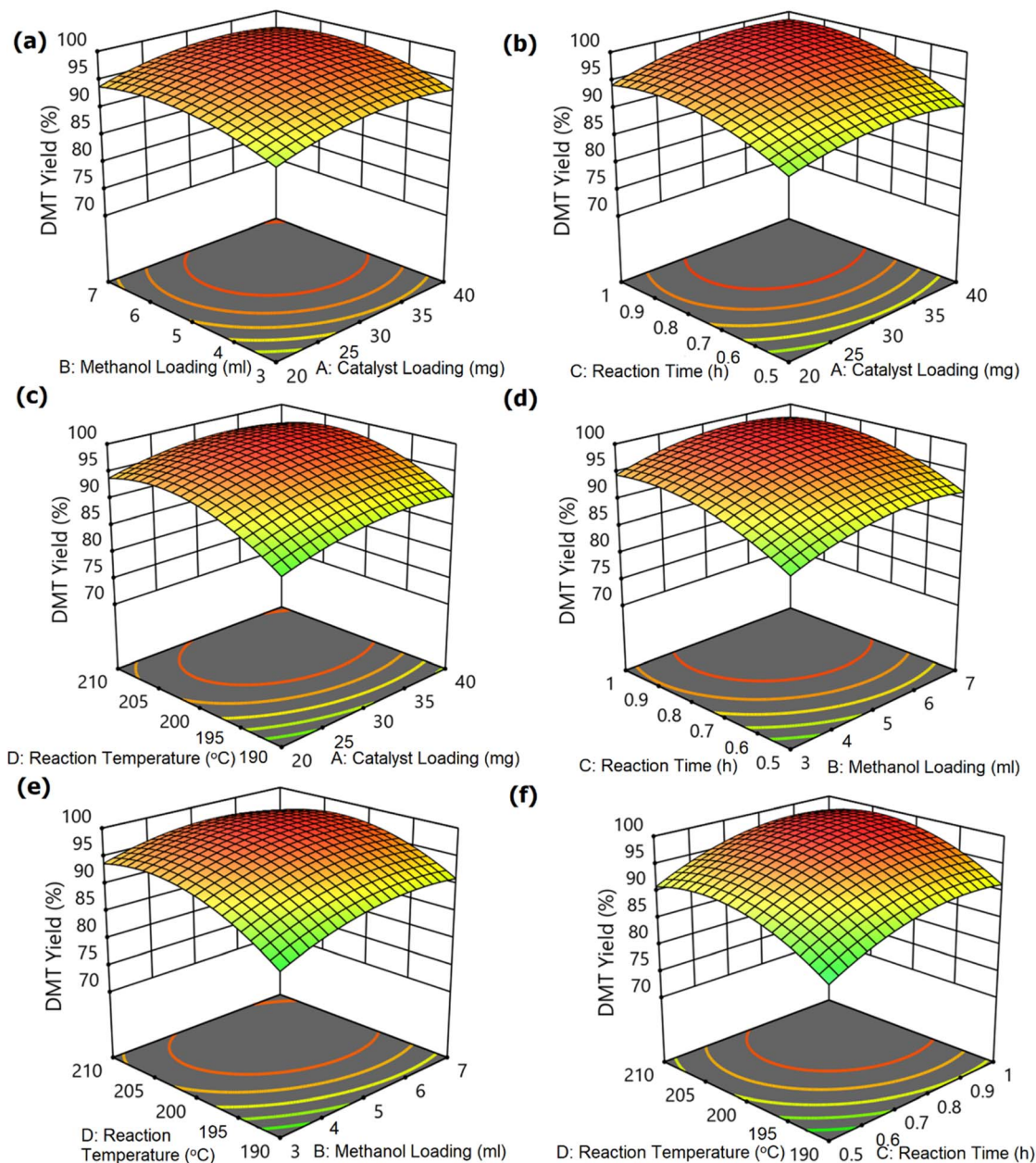Fig. 2   (a) Predicted vs. actual yield plot. (b) Normal plot of residuals.

Fig. 3 (a) Methanol loading (mL) *vs.* catalyst loading (mg). (b) Reaction time (h) *vs.* catalyst loading (mg). (c) Reaction temperature (°C) *vs.* catalyst loading (mg). (d) Reaction time (h) *vs.* methanol loading (mL). (e) Reaction temperature (°C) *vs.* methanol loading (mL). (f) Reaction temperature (°C) *vs.* reaction time (h).

yield of 99.65% using 36.29 mg catalyst loading and 5.7 mL methanol loading at 204 °C reaction temperature and 0.97 h reaction time. The predicted optimal conditions were then experimentally validated in triplicate, yielding 98.64 ± 0.11% DMT, residing within the confidence interval of 98.26–101.06%. Thus, the above condition was confirmed as the optimum condition to provide the maximum yield of DMT. The pressure generated inside the reactor under the optimized conditions was estimated to be ∼4.072 MPa, calculated using the NIST Antoine equation (see SI page 7).[51,52]

The crude product was subjected to HPLC analysis, and the finding revealed the presence of bis(2-hydroxyethyl)terephthalate (BHET), ethylene glycol (EG), and 2-hydroxyethyl methyl tere-phthalate (HEMT), other than DMT from their corresponding retention times of 1.945, 3.338, 4.429, and 7.556, respectively, as shown in Fig. S24.[53] However, as shown in Fig. S25, the recrys-tallized product was free from BHET, HEMT, and EG.

The recrystallized DMT was further analyzed with FT-IR spectroscopy to validate the functional group (see Fig. S19). The carbonyl group C=O of the ester was found to exist at 1712 cm^{-1}, and the C–O and C–O–C stretching vibrations of the ester were also observed at 1265 cm^{-1} and 1103 cm^{-1}. Moreover, the exis-tence of the methyl group can also be seen at 2962 cm^{-1}, and these all correspond to the structural properties of DMT.

^{1}H and ^{13}C NMR analysis was further performed for structural confirmation. The distinct peaks shown in Fig. 4 signify the presence of different proton environments in the sample. The ^{1}H NMR spectrum of dimethyl terephthalate (DMT) (Fig. 4) shows distinct peaks corresponding to different proton environments in the molecule. Residual DMSO-d_6 solvent caused a peak at 2.5 ppm, while a trace amount of moisture in the sample may have caused a peak at $\delta = 3.3$ ppm. The methoxy protons (–OCH$_3$) of the ester groups show a peak at $\delta = 3.9$ ppm, and the aromatic protons of the terephthalate ring resonate at $\delta = 8.0$ ppm. Moreover, the singlet peaks at $\delta = 52.95$ and 165.94 ppm in the ^{13}C NMR spectra (Fig. S20) correspond to methoxy and carbonyl carbons, while peaks at $\delta = 129.92$ and 133.94 ppm can be assigned to aromatic carbons. These peaks confirm the successful formation of the desired dimethyl terephthalate (DMT) product, consistent with its expected structural features.

6. Leaching and reusability test of the catalyst

ICP-OES analysis reveals the leaching of calcium and potassium at concentrations of 0.5256 mg L^{-1} and 90.468 mg L^{-1}, respectively. However, the methanolysis test conducted using the leachate produced only 1.8% DMT yield, indicating that the dissolved metal species exhibit negligible catalytic activity. This confirms that the reaction is predominantly catalyzed by the solid heterogeneous catalyst.

The catalyst's reusability was systematically evaluated over ten consecutive cycles under identical reaction conditions without any additional activation treatment. A weight loss of $\sim$6–10 wt% was observed after each recovery; however, no fresh catalyst was added to compensate for this loss. Instead, the PET loading and other reaction components were proportionally adjusted based on the quantity of the recovered catalyst, as discussed in the experimentation section. After each run, the catalyst was simply washed with hot methanol and dried at 80 °C for one hour. A gradual increase in reaction time accompanied by a slight decline in DMT yield was observed over successive cycles (Table S2). In the second cycle, the reaction required approximately two additional minutes compared to the first, with a $\sim$2% reduction in DMT yield. This trend continued with minor fluctuations, reaching 91% yield in the fifth cycle with a reaction time of 2 h, indicating excellent stability and sustained catalytic activity.

The observed changes in yield and reaction time are primarily attributed to the leaching of active sites, particularly potassium (10.28 wt% loss), as revealed by EDX elemental analysis (Fig. S21). Upon extending the reusability study to the 10th cycle, the reaction time increased to 2.9 h, and the DMT yield decreased to 84.56% (Table S2). Further potassium leaching of approximately 2.8 wt% was detected (Fig. S22), while no significant morphological alterations were observed (Fig. S23).[50]

These results collectively demonstrate that, although partial leaching of active components occurs during repeated use, the
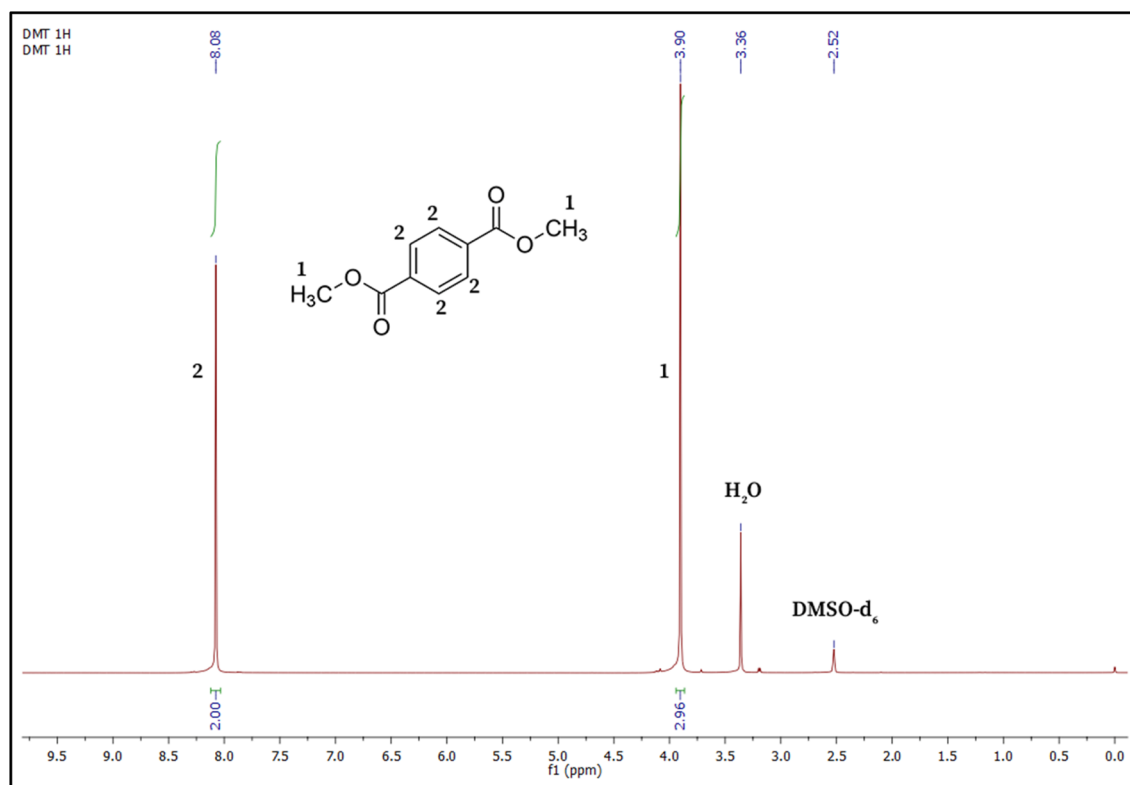

Fig. 4 ^{1}H NMR spectra of the recrystallized methanolysis product (DMT).

© 2026 The Author(s). Published by the Royal Society of Chemistry

Environ. Sci.: Adv., 2026, **5**, 192–205 | **201**

solid catalyst retains considerable activity and structural integrity, even after ten consecutive reaction cycles, underscoring its robustness and potential for practical application in PET methanolysis.

7. Energy input, mass balance, and green metrics of the methanolysis reaction

The specific energy consumption for the production of DMT was initially determined under the optimized conditions, resulting in a high value of 5286.14 kWh kg^{-1}. However, this value progressively decreases as the PET loading and corresponding reaction components (methanol and catalyst) are increased up to the operational limits of the available equipment, as shown in Table S4, entry B, 1–4. This finding reveals that the energy consumption depends on the initial PET charge and the reactor's capacity. To validate this observation, a theoretical estimation was conducted for a 1 kg PET loading. Although this larger-scale operation requires a longer setting time to initiate the reaction and evaporation, it resulted in a significantly lower energy consumption of 46.66 kWh kg^{-1} – a dramatic reduction from the 5286.14 kWh kg^{-1} obtained for 0.5 g PET depolymerization. Under the optimized conditions, the mass balance for each component – DMT, byproducts, ethylene glycol, recovered methanol, and the total mass loss – was determined to be 0.498 g, 0.0045 g, 0.147 g, 3.84 g, and 0.54 g, respectively, as shown in Table S6. Additionally, the green metrics such as E-factor and PMI were determined to be 1.06 and 2.06, respectively (see Table S5), demonstrating the high efficiency and environmental favorability of the process.[54,55]

8. Depolymerization of colored and labeled PET

The robustness of the catalyst was further evaluated using blue, green, and red (UV-blocked) PET flakes, as well as labeled postconsumer PET, under the optimized reaction conditions, with all experiments performed in triplicate. The recrystallized DMT yield from colored PET bottles was found to be slightly lower than that from clear PET, with no significant variation among the different colors, as presented in Table S3. This minor reduction can be attributed to the additional washing steps required to remove the colored solution. In the case of labelled PET, the yield was 91.52 ± 0.58%, which is relatively low compared to the clear PET. However, full conversion of PET was observed for all samples, including labelled and pigmented, within the optimum reaction time of 0.97 h. The reduced yield for labelled PET is primarily attributed to the label material adhering to the PET flakes. Furthermore, the UV spectra of all recrystallized DMT shown in Fig. S29 confirm the complete removal of added colors. These results demonstrate that DFPA exhibits high tolerance to impurities, including pigments, UV-blocking additives, and labels.

9. Plausible mechanistic insights into PET methanolysis using DFPA

The methanolysis reaction proceeds through a base-catalyzed solid–liquid–solid transesterification pathway, wherein PET (solid substrate) is depolymerized by methanol in the presence of a heterogeneous DFPA catalyst, without the need for mechanical stirring. The basic sites, predominantly O^{2-} originating mainly from K$_2$O, CaO, MgO, etc., abstract a proton from the methanol to generate reactive methoxide ions. These methoxide ions then serve as a key nucleophile that attacks the electrophilic carbon of the ester bonds in PET to form a tetrahedral intermediate. Subsequent rearrangement of this intermediate then regenerates C=O, cleaving the ester linkage to form oligomers, dimers, and monomeric dimethyl terephthalate together with ethylene glycol.[50] In the meantime, HPLC analysis revealed the presence of a reversible equilibrium, resulting in the formation of intermediates such as bis(2-hydroxyethyl)terephthalate and hydroxyethyl methyl terephthalate.

10. Relative comparison of the DFPA catalyst with recently reported literature between 2022 and 2025

Recent advances (2022–2025) in PET methanolysis have introduced a variety of catalysts, ranging from homogeneous to heterogeneous systems, many of which exhibit excellent

Table 7 Comparative data of the proposed catalyst with recently published catalysts

Sl./no.	Catalyst	Catalyst nature	Reaction conditions	Recyclability cycle	DMT yield	Reference
1	[HN$_{222}$·N$_{222}$][HSO$_4$]	Ionic liquids	200^a, 1 : 75^b, 3 h, 180 °C	5^c, 46%	97%	56
2	[EMIm][OAc]	Ionic liquids	5^a, 1 : 1.3^b, 2.5 h, 130 °C	Nil	99%	57
3	Zn(OAc)$_2$·2H$_2$O	Homogeneous catalyst	0.2^d, 1 : 6 : 4^e, 2 h, 150 °C, 0.9 MPa	Nil	97.8%	58
4	Zn-Beta-meso	Heterogeneous catalyst	20^d, 1 : 800^b, 30 min, 180 °C, 3 MPa of N$_2$	5^c, 91%	>99%	59
5	BLA	Heterogeneous catalyst	20.8^d, 1 : 49^b, 2 h, 200 °C	4^c, 67.01%	78%	50
6	OPA@Fe$_3$O$_4$	Heterogeneous catalyst	4^d, 1 : 49^b, 4 h, 200 °C	10^c, 70%	83%	53
7	MgO/NaY	Heterogeneous catalyst	4^d, 1 : 6^f, 30 min, 200 °C	6^c	91%	60
8	DFPA	Heterogeneous catalyst	7.5%^{d}, 1 : 49^b, 0.9 h, 200 °C, 3.78 MPa	10^c, 84.56%	98.64%	This work

^{a} Catalyst loading (mol%). ^{b} PET to methanol molar ratio. ^{c} Number of cycles. ^{d} Weight percentage. ^{e} PET to γ-valerolactone (co-solvent) to methanol mass ratio. ^{f} PET to methanol mass ratio.

activity, but differ in performance characteristics and possess certain limitations compared to the present catalyst, as shown in Table 7. For instance, ionic liquids such as $[HN_{222}\cdot N_{222}]$ $[HSO_4]$ and $[EMIm][OAc]$ achieved high DMT yields of 97% and 99%, respectively. However, the former requires higher dosages of several important parameters (excluding reaction temperature) and offers limited recyclability, while the latter, despite showing superior performance in most parameters, lacks reusability and requires a longer reaction time (2.5 h). Similarly, the single-use nature of the homogeneous $(Zn(OAc)_2\cdot 2H_2O)$ catalyst limits it practical usage in large-scale production, despite its good performance under relatively mild conditions. Among the four solid catalysts examined, only the Zn-Beta-meso catalyst competes with DFPA in terms of DMT yield, but it requires relatively higher amounts of both catalyst and methanol. In contrast, DFPA demonstrates superior practicality and sustainability, delivering consistently good yield even after the 10th cycle, with only a minimal catalyst loss of 6–10% per cycle.

11. Conclusion

A bio-waste-derived DFPA catalyst exhibited remarkable bifunctional catalytic activity, effectively promoting both the Michael addition reaction and the methanolysis of polyethylene terephthalate (PET) waste. Notably, all sixteen model Michael addition reactions achieved complete conversion within a short reaction time using only 10 wt% of the catalyst, highlighting its efficiency and broad substrate applicability. While recent advances in Michael addition catalysts have reported good to excellent yields,[61–65] the complex synthesis procedures of many of these catalysts hinder their practical applicability compared to the environmentally benign, cost-effective, abundantly available, and renewable DFPA catalyst. Furthermore, the catalyst enabled full conversion of PET under optimized methanolysis conditions, which were systematically determined using central composite design-based response surface methodology (CCD-RSM). The statistical robustness of the experimental model was confirmed using analysis of variance (ANOVA). The optimal conditions – 204 °C, 0.97 h reaction time, 36.29 mg of catalyst, and 5.7 mL of methanol – resulted in a high recrystallized yield of dimethyl terephthalate (DMT) at 98.64%. Despite a gradual decline to 91.46% yield by the fifth cycle, particularly with increased reaction time, the catalyst retained substantial activity, underscoring its potential for repeated use up to the 10th cycle. The green metrics of both the reactions demonstrated significant environmental savings, and these findings position the DFPA heterogeneous catalyst as a promising, sustainable alternative to conventional catalysts in advancing green chemistry and integrated waste valorization strategies.

Ethical statement

This work did not require ethical approval from a human subject or animal welfare committee.

Author contributions

Vanlalngaihawma Khiangte: methodology, experimentation, formal analysis, writing – original draft, review, and editing; Samson Lalhmangaihzuala: data analysis, writing – original draft, review, and editing; Z. T. Laldinpuii: investigation, validation, writing – review and editing; K. Vanlaldinpuia: methodology, conceptualization, funding acquisition, resources, supervision, writing – review and editing.

Conflicts of interest

There are no conflicts to declare.

Data availability

The catalyst characterization data and analytical details are available at **https://doi.org/10.1016/j.biteb.2023.101663**.

The additional data supporting this article are provided as part of the supplementary information (SI), and the raw data such as BET, HPLC, NMR, SEM, TEM, TGA, XPS, XRD, XRF, energy input, FT-IR, ICP-OES, mass balance and green metrics, RSM DXPS file, TPD, and the Origin software file containing the UV spectra of colored PET are available at **https://data.mendeley.com/datasets/zmx9mh7h9y/1**. Supplementary information is available. See DOI: **https://doi.org/10.1039/d5va00253b**.

Acknowledgements

References

1 T. Espinoza-Tellez, J. B. Montes, R. Quevedo-León, E. Valencia-Aguilar, H. Aburto Vargas, D. Díaz-Guineo, M. Ibarra-Garnica and O. Díaz-Carrasco, *Sci. Agropecu.*, 2020, **11**, 427–437.

2 A. R. Shafqat, M. Hussain, Y. Nawab, M. Ashraf, S. Ahmad and G. Batool, *Int. J. Polym. Sci.*, 2023, **2023**, 5872605.

3 G. Weldesemayat Sileshi, E. Barrios, J. Lehmann and F. N. Tubiello, *Earth Syst. Sci. Data*, 2025, **17**, 369–391.

4 J. A. Bennett, K. Wilson and A. F. Lee, *J. Mater. Chem. A*, 2016, **4**, 3617–3637.

5 C. O. Tuck, E. Pérez, I. T. Horváth, R. A. Sheldon and M. Poliakoff, *Science*, 2012, **337**, 695–699.

6 C. S. K. Lin, L. A. Pfaltzgraff, L. Herrero-Davila, E. B. Mubofu, S. Abderrahim, J. H. Clark, A. A. Koutinas, N. Kopsahelis, K. Stamatelatou, F. Dickson, S. Thankappan, Z. Mohamed,

© 2026 The Author(s). Published by the Royal Society of Chemistry

Environ. Sci.: Adv., 2026, **5**, 192–205 | **203**

R. Brocklesby and R. Luque, *Energy Environ. Sci.*, 2013, **6**, 426–464.

7 B. Scott, A. H. Baldwin and S. A. Yarwood, *Biogeosciences*, 2022, **19**, 1151–1164.

8 V. Strokal, A. Kurovska and M. Strokal, *J. Integr. Environ. Sci.*, 2023, **20**, 2281920.

9 L. Chanduka and R. Pal Singh, *J. Pollut. Eff. Cont.*, 2015, **4**, 1000150.

10 M. Phogat, R. Dahiya, P. Sangwan and A. Addy, *Int. J. Chem. Stud.*, 2020, **8**, 2534–2538.

11 P. Rudziak, E. Batung and I. Luginaah, *PLoS One*, 2024, **19**, e0300801.

12 K. Lee, Y. Jing, Y. Wang and N. Yan, *Nat. Rev. Chem.*, 2022, **6**(9), 635–652.

13 R. Nkoa, *Agron. Sustainable Dev.*, 2014, **34**, 473–492.

14 C. Du, S. Munir, R. Abad and D. Lu, *Waste Biorefinery: Integrating Biorefineries for Waste Valorisation*, ed. T. Baskar, A. Pandey, E. R. Rene and D. C. W. Tsang, Elsevier, Amsterdam, 2020, vol. 7, ch. 1, pp. 179–198.

15 C. Voruganti, *Environ. Rep.*, 2023, **5**, 1–4.

16 M. S. Kim, H. Chang, L. Zheng, Q. Yan, B. F. Pfleger, J. Klier, K. Nelson, E. L. W. Majumder and G. W. Huber, *Chem. Rev.*, 2023, **123**, 9915–9939.

17 S. H. Y. S. Abdullah, N. H. M. Hanapi, A. Azid, R. Umar, H. Juahir, H. Khatoon and A. Endut, *Renewable Sustainable Energy Rev.*, 2017, **70**, 1040–1051.

18 H. He, R. Zhang, P. Zhang, P. Wang, N. Chen, B. Qian, L. Zhang, J. Yu and B. Dai, *Adv. Sci.*, 2023, **10**, 2205557.

19 K. Saikia, A. Das, A. H. Sema, S. Basumatary, N. Shaemningwar Moyon, T. Mathimani and S. L. Rokhum, *Renewable Energy*, 2024, **229**, 120743.

20 S. Ao, S. P. Gouda, M. Selvaraj, R. Boddula, N. Al-Qahtani, S. Mohan and S. L. Rokhum, *Energy Convers. Manage.*, 2024, **300**, 117956.

21 K. Rajkumari, D. Das, G. Pathak and L. Rokhum, *New J. Chem.*, 2019, **43**, 2134–2140.

22 Z. T. Laldinpuii, C. Lalmuanpuia, S. Lalhmangaihzuala, V. Khiangte, Z. Pachuau and K. Vanlaldinpuia, *New J. Chem.*, 2021, **45**, 19542–19552.

23 I. Yunita, S. Putisompon, P. Chumkaeo, T. Poonsawat and E. Somsook, *Chem. Pap.*, 2019, **73**, 1547–1560.

24 S. Lalhmangaihzuala, Z. Laldinpuii, C. Lalmuanpuia and K. Vanlaldinpuia, *Polymers*, 2021, **13**, 37.

25 Z. Laldinpuii, S. Lalhmangaihzuala, Z. Pachuau and K. Vanlaldinpuia, *Waste Manage.*, 2021, **126**, 1–10.

26 A. Abbas, L. T. Mariana and A. N. Phan, *Carbon*, 2018, **140**, 77–99.

27 V. Khiangte, S. Lalhmangaihzuala, Z. T. Laldinpuii, L. Nunnemi, R. B. Muthukumaran and K. Vanlaldinpuia, *Bioresour. Technol. Rep.*, 2023, **24**, 101663.

28 I. B. Laskar, T. Deshmukhya, A. Biswas, B. Paul, B. Changmai, R. Gupta, S. Chatterjee and S. L. Rokhum, *Energy Adv.*, 2022, **1**, 287–302.

29 I. B. Laskar, R. Gupta, S. Chatterjee, C. Vanlalveni and L. Rokhum, *Renewable Energy*, 2020, **161**, 207–220.

30 H. Chen, K. Wan, Y. Zhang and Y. Wang, *ChemSusChem*, 2021, **14**, 4123–4136.

31 Y. L. Wang, Y. H. Lee, I. J. Chiu, Y. F. Lin and H. W. Chiu, *Int. J. Mol. Sci.*, 2020, **21**, 1727.

32 A. Bohre, P. R. Jadhao, K. Tripathi, K. K. Pant, B. Likozar and B. Saha, *ChemSusChem*, 2023, **16**, e202300142.

33 L. I. Putman, L. G. Schaerer, R. Wu, D. G. Kulas, A. Zolghadr, R. G. Ong, D. R. Shonnard and S. M. Techtmann, *Microbiol. Spectrum*, 2023, **11**, e00362.

34 M. J. Kang, H. J. Yu, J. Jegal, H. S. Kim and H. G. Cha, *Chem. Eng. J.*, 2020, **398**, 125655.

35 E. Barnard, J. J. Rubio Arias and W. Thielemans, *Green Chem.*, 2021, **23**, 3765–3789.

36 M. Han, *Recycl. Polyethylene Terephthalate Bottles*, 2019, 85–108.

37 P. J. Deuss, K. Barta and J. G. De Vries, *Catal. Sci. Technol.*, 2014, **4**, 1174–1196.

38 R. Mahrwald, *Drug Discovery Today: Technol.*, 2013, **10**, e29–e36.

39 N. G. Schmidt, E. Eger and W. Kroutil, *ACS Catal.*, 2016, **6**, 4286–4311.

40 S. Lalhmangaihzuala, V. Khiangte, Z. Laldinpuii, L. Nunnemi, J. Malsawmsanga, G. Lallawmzuali, T. Liana, C. Lalhriatpuia, Z. Pachuau and K. Vanlaldinpuia, *Chemistry*, 2023, **5**, 2362–2375.

41 O. Baslé, W. Raimondi, M. D. M. S. Duque, D. Bonne, T. Constantieux and J. Rodriguez, *Org. Lett.*, 2010, **12**, 5246–5249.

42 K. D. Nguyen, C. Kutzscher, F. Drache, I. Senkovska and S. Kaskel, *Inorg. Chem.*, 2018, **57**, 1483–1489.

43 C. Palomo, S. Vera, A. Mielgo and E. Gómez-Bengoa, *Angew. Chem., Int. Ed.*, 2006, **45**, 5984–5987.

44 O. M. Berner, L. Tedeschi and D. Enders, *Eur. J. Org. Chem.*, 2002, **2002**, 1877–1894.

45 T. Das, S. Mohapatra, N. P. Mishra, S. Nayak and B. P. Raiguru, *ChemistrySelect*, 2021, **6**, 3745–3781.

46 T. I. Crowell and T. rin Kim, *J. Am. Chem. Soc.*, 1973, **95**, 6781–6786.

47 C. F. Bernasconi and P. Paschalis, *J. Am. Chem. Soc.*, 1989, **111**, 5893–5902.

48 N. Chumuang and V. Punsuvon, *J. Chem.*, 2017, **2017**, 4190818.

49 S. P. Gouda, J. M. Jasha, P. Kumar, A. Dhakshinamoorthy, U. Rashid and S. L. Rokhum, *Catalysts*, 2022, **12**, 1312.

50 Z. T. Laldinpuii, V. Khiangte, S. Lalhmangaihzuala, C. Lalmuanpuia, Z. Pachuau, C. Lalhriatpuia and K. Vanlaldinpuia, *J. Polym. Environ.*, 2022, **30**, 1600–1614.

51 D. Ambrose, C. H. S. Sprake and R. Townsend, *J. Chem. Thermodyn.*, 1975, **7**, 185–190.

52 P. Moshele, M. R. Stenzel, D. Drolet and S. F. Arnold, *Ann. Work Exposures Health*, 2024, **68**, 409–419.

53 S. Lalhmangaihzuala, Z. T. Laldinpuii, V. Khiangte, G. Lallawmzuali, Thanhmingliana and K. Vanlaldinpuia, *Adv. Powder Technol.*, 2023, **34**, 104076.

54 R. A. Sheldon, *Green Chem.*, 2017, **19**, 18–43.

55 R. A. Sheldon, *ACS Sustain. Chem. Eng.*, 2017, **6**, 32–48.

56 E. McCrea, P. Goodrich, J. D. Holbrey and M. Swadźba-Kwaśny, *RSC Sustainability*, 2025, **3**, 3987–3996.

57 M. Zhang, Y. Lu, Z. Wang, X. Gao, X. Luo, X. Shen, W. Wu and Q. Mei, *Eco-Environ. Health*, 2025, **4**, 100139.

58 Z. Ding, X. Cao, X. Y. Hao and Y. P. Ni, *Polymers*, 2025, **17**, 1458.

59 X. Mu, D. Lin, J. Zhang, X. Qin, J. Huang and F.-S. Xiao, *Carbon Future*, 2025, **2**, 9200039.

60 S. Tang, F. Li, J. Liu, B. Guo, Z. Tian and J. Lv, *J. Environ. Chem. Eng.*, 2022, **10**, 107927.

61 X. H. Xu, R. T. Gao, S. Y. Li, L. Zhou, N. Liu and Z. Q. Wu, *Chem. Sci.*, 2024, **15**, 12480–12487.

62 P. R. Sharma, A. Malik, S. Bandaru, K. Vashisth, N. K. Rana and R. K. Sharma, *Chem. Commun.*, 2022, **58**, 7249–7252.

63 H. Zhao, A. Roy, A. Samaranayake, P. Ishtaweera, G. A. Baker, N. Duong, L. G. Markmann, N. S. Fernando and K. R. Mitchell-Koch, *Langmuir*, 2025, **41**, 12718–12730.

64 J. H. Shim, S. H. Cheun, H. S. Kim and D. C. Ha, *Molecules*, 2022, **27**, 2759.

65 F. Ghobakhloo, D. Azarifar, M. Mohammadi, H. Keypour and H. Zeynali, *Inorg. Chem.*, 2022, **61**, 4825–4841.

© 2026 The Author(s). Published by the Royal Society of Chemistry

Environ. Sci.: Adv., 2026, **5**, 192–205 | 205